A broad perspective on automated CME Tracking: towards higher level space weather forecasting

E. Robbrecht and D. Berghmans
(Eva.Robbrecht@oma.be)

SIDC - Royal Observatory of Belgium
Ringlaan 3, 1180 Brussel, Belgium

Received: 28 Feb 2005 / Accepted: 04 Nov 2005

Abstract

We discuss our current capabilities to deliver the CME parameters required for the space weather forecasting process. The ever growing importance of space weather has lead to new requirements on the timeliness and objectiveness of CME detection. It has become indispensable to report the occurrence of Earth-directed CMEs and to predict their possible impact on the geospace environment. Early 2005, we are on the eve of a new era in space weather forecasting. We point out the restricted accuracy on the current forecasts and discuss a chance for amelioration. This invokes data-driven models (empirical and numerical), triggered by a real-time CME disturbance, simulating the propagation and interaction of the ejection with the ambient solar wind. We discuss the link between the direct observable parameters (like the CME *projected* speed and angle around the occulter) and the required input parameters (like radial speed, direction, ...). The only way to guarantee the real-time value of the simulations is by employing software which autonomously detect CME parameters in a variety of data. This paper focusses on the automated CME detection algorithms that are currently available. Automated CME tracking is yet in its infancy, therefore this 'review' will be an outlook on the potential of this field rather than looking back on already achieved milestones.

1 Introduction

Since their discovery in the seventies in coronagraphic observations on the OSO-7 sattelite (Tousey et al. 1974) and the Skylab mission (Gosling et al. 1974) coronal mass ejections have been subject to numerous studies. Recent reviews can be found in Forbes (2000); Low (2001); Low & Zhang (2002). With the increase in knowledge on the physics of CMEs, there has also been an increase in the number of ways a CME can be observed. CMEs are now known to be complex events linked to other phenomena such as flares and filament/prominence eruptions; however also more subtle events like dimmings, EIT waves and radio type II bursts are valuable CME indicators. For reviews on the different CME manifestations and related events we refer to Hudson & Cliver (2001); Cliver & Hudson (2002); Munro et al. (1979). *In situ*, the passage of an interplanetary CME (ICME) appears as a shock in the solar wind parameters. They are generated by compressive interaction regions formed as the CME overtakes slower plasma (Gosling et al. 1994). CMEs are the most energetic eruptions on the Sun, are the primary cause of major geomagnetic storms and are believed to be responsible for the largest solar energetic particle events (Gosling et al. 1990; Tsurutani et al. 1997). These events can highly affect radio HF communication throughout the polar region (no other communication is possible above 82 degrees latitude, e.g. for polar flights), the reliability of power systems (voltage control problems, blackout or collapse of grid, damage to transformers), induce currents on pipelines and cause spacecraft surface charging. Hence, to guarantee the reliability of many technologically dependant systems and activities, timely and accurate forecasting of the most energetic space weather events - CMEs - have become indispensable. A good forecast includes information on the onset time, the duration and the strength of the storm. In order to allow companies to take protective action in preparation of the storm, this forecast should be done as timely as possible. Unlike terrestrial weather conditions, which are monitored routinely at thousands of locations around the world, the conditions in space are monitored by only a handful of space-based and ground-based facilities. Space weather forecasters are required to predict conditions in space and on Earth using a very limited guidance from actual measurements.

From the moment an indication for CME occurrence is observed, space weather forecasters try to gather as much details as possible on the nature, origin and evolution of the CME. This involves usually combined observations in the EUV and X-rays as well

as coronagraphic movies, magnetograms and irradiance data. Given the occurrence of a CME, the main task of a space weather forecaster is to predict if, when, for how long and how strong it will impact the earth. Translated in terms of *in situ* data, this means we need to estimate the solar wind speed and density and the north-south orientation of the IMF (B_z), since these are the most important parameters deciding the geo-efficiency (recent studies are Gopalswamy 2003; Yurchyshyn et al. 2003, 2004; Zhang et al. 2004) . Two stages can be discerned in the forecasting process. Using remote sensing data one can obtain a 2-4 day warning time (depending on the speed of the CME) with rough estimations on the CME time of arrival and the expected impact. This is done by assigning probabilities on the future geomagnetic activity levels. When the perturbation induced by the CME actually passes by at L1 (215 $R_\odot$) new *in situ* data becomes available (ACE, CELIAS onboard SOHO , Wind when available) allowing amelioration of the forecast $\sim$ 1 hour ahead of the magnetospheric disturbances. It is obvious that this data gap between 32 (LASCO field-of-view) and 215 $R_\odot$ makes accurate forecasting only possible on the short term. The challenge for space weather forecasting is to enhance the accuracy of the forecast 2-4 days before the onset of the storm despite the limited amount of data available. New types of remote sensing instruments make it in principle possible to observe CMEs continuously from the Sun till 1 AU: SMEI, (Solar Mass Ejection Imager Eyles et al. 2003), the Heliospheric Imagers (HI Defise et al. 2001) onboard STEREO (Solar Terrestrial Relations Observatory) or interplanetary scintillation techniques (IPS Watanabe & Schwenn 1989). These instruments are however far from being usable in an operational context.

The vision for future space weather forecasting (illustrated in Fig. 1) is to utilize a sequence of real-time data-driven models that simulate the CME evolution from the Sun via L1 to the Earth and eventually calculating its effect on the geo-space. Ideally, heliospheric models should deliver *in situ*-like parameters quantifying the perturbation at L1 like the solar wind speed, density, temperature and magnetic field parameters, which can on their turn serve as input for magnetospheric and ionospheric models. This will allow the formulation of a more accurate 2-4 day forecast. Hence, CME surveillance implies identifying CME parameters, which can serve as input for CME propagation models. To describe a CME and its interaction with background solar wind as completely and correctly as possible there is the need to assimilate all relevant data (magnetograms, EUV movies, coronagraphic sequences, radio observations). The only way to extract the required CME parameters from these data in near-real-time is by integrating automated software in the forecasting process. This appears to be the best approach to significantly improve space weather forecasting in the near future.

In this paper we focus on the current status of the *automated nowcast capabilities of the various CME manifestations*. In the next section we illustrate the model-for forecast principle enlisting existing efforts. We argue that the next step includes CME driven models predicting its manifestation at 1 AU. We compare the directly measured parameters with the needed input parameters. In section 3 we discus the available algorithms for automated CME detection which are needed to ensure the timeliness of the required data.

2 The model-for-forecast principle

The concept of real-time data-driven modelling is young but not new. At the NOAA-SEC Rapid Prototyping Center (RPC, http://www.sec.noaa.gov/rpc/), various models are tested on their operational use. However, up till now it has been common to use measurements form the Lagrangian point (L1) to drive magnetospheric and ionospheric forecast models. These allow accurately forecasting the upcoming geomagnetic activity during the next few hours, but not the next few days. In order to enhance the quality of the 2-4 day forecasts we should focus on integrating heliospheric models in the forecasting process. Modeling a CME event from the sun to the Earth is a complex task. Even starting from above the barely understood CME initiation, modeling the evolution, propagation and interaction of a CME with the background solar wind is a big challenge.

A new approach to this problem is the coupled-model approach, adopted and assessed by the Center for Integrated Space weather Modeling (CISM Spence et al. 2004). The CISM simulate the Sun-Earth system by coupling state-of-the-art codes modeling the solar corona, solar wind, magnetosphere and upper atmosphere/ionosphere using interfaces that exchange parameters specifying each component of the solar-terrestrial system. In addition, new efforts involve techniques continuously assimilating new data to keep the forecast 'on track'. As to proof the coupled-model-for-forecasting principle Luhmann et al. (2004) have simulated a Sun-to-Earth space weather event from the Solar corona to the Earth's ionosphere. Many recent examples of modeling space weather events from the Sun to 1 AU (L1 or Earth) exit (e.g. Wu & Guo 1999; Odstrcil et al. 2004; Manchester et al. 2004; Intriligator et al. 2005).

Given the challenge to produce effective and efficient phys-ics based models, forecasters now mostly rely on empirical models based on large statistics. The information extracted from these models is mostly restricted to kinematic properties (speed, acceleration, travel time), given the assumption of an

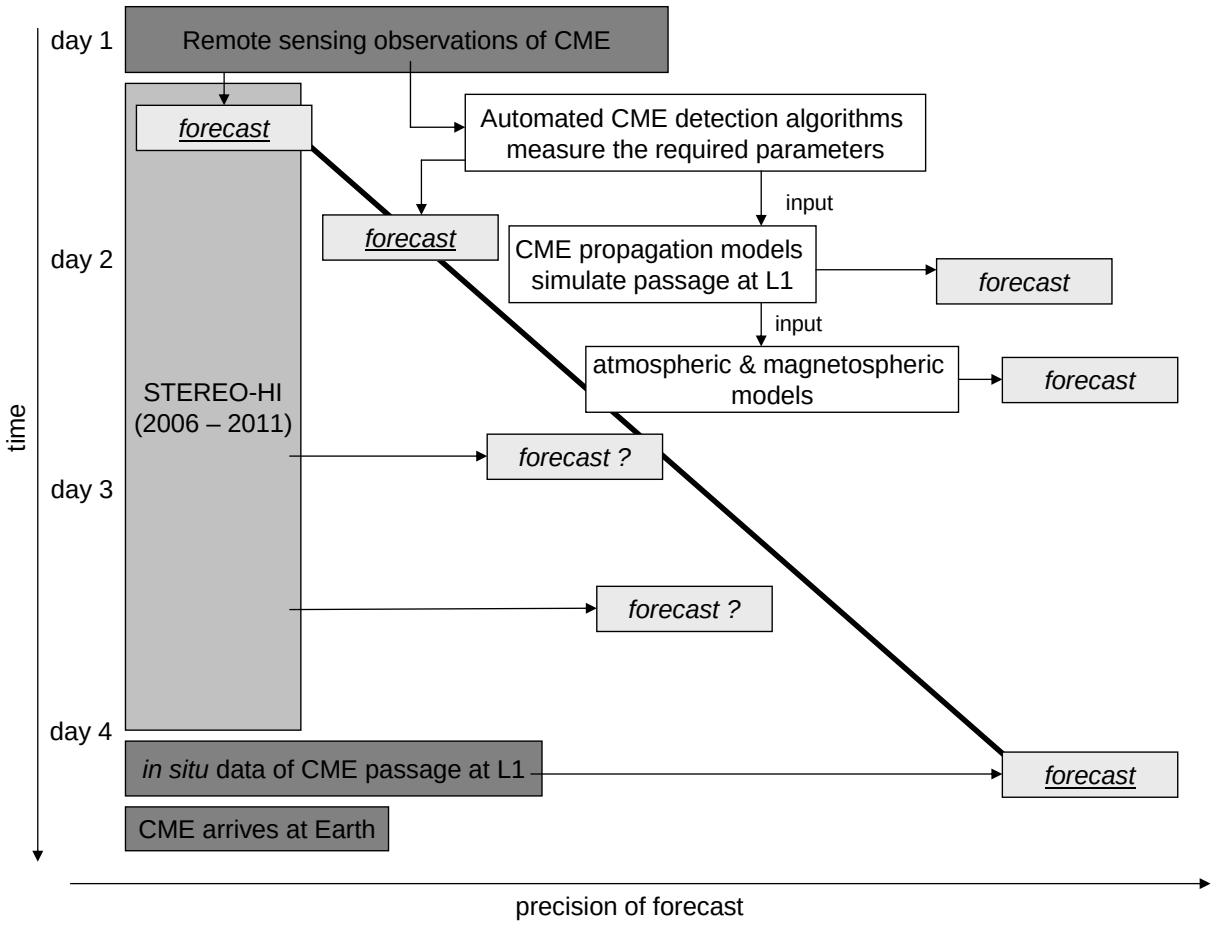

Figure 1: Concept map illustrating the value of real-time data-driven models regarding space weather forecasting. The vertical bar indicates the timeline. Note the current gap of new data between day 1 and day 4 (for example). This is expected to be filled with STEREO data in 2006. The horizontal bar indicates the precision of the forecast. The more to the right, the more reliable is the forecast. With the current data limitation to 30 $R_{\odot}$, only better understanding and models simulating the CME evolution from the Sun to L1 can push the forecast to the right. The underlined forecasts represent the actual forecasting process.

earth directed CME. Despite their limited accuracy and information, they are of great value for forecasters and as reference models against which the newly developed models are compared. Recent examples of such an empirical approach are found in dal Lago et al. (2003); Xie et al. (2004); Gopalswamy et al. (2005). The strength of the empirical model is its operational simplicity and therefore its ability to make quickly a good *estimate* of the arrival of a CME. The more advanced empirical models do even incorporate ambient parameters, like the average solar wind speed ($\sim$ 400 km s^{-1}). Numerical models are expected to be slightly better in predicting arrival times of CMEs, because they can use more realistic ambient solar wind. Further, numerical simulations provide global context, predictions whether shock and/or ejecta will arrive to Earth and also are expected to predict the connectivity of the IMF line between Earth and eventual shock (Odstrcil et al. 2004).

Directly connected to the call for inputs, there is the question of the operational capacity to deliver these parameters and with what accuracy and timeliness. At present our capacity to measure the time-dependent boundary-conditions near the sun are very limited. Therefore various approximations are utilized. CMEs are classically viewed with coronagraphs in space above the scattered light form the Earth's atmosphere. The observed white light signal is roughly proportional to the integrated mass along the line of sight. Ironically, the most geo-effective CMEs (halo and partial halo CMEs) are the most difficult to measure: they are very faint (due to Thomson scattering and a short integration length in the line of sight direction) and their structure is often very complicated. Measurements of the CME's *projected* speed, launch-angle and mass can be deduced from this data.

We need thus an 'interface' translating the measured parameters into input-parameters. Schwenn et al. (2001) have introduced the 'lateral expansion speed' of a CME and derived its relation with the radial speed (dal Lago et al. 2003). Under the assumption that halo CMEs propagate radially and with constant angular widths, Zhao et al. (2002) can reproduce some useful geometric and kinematic properties of halo CMEs using a simple geometrical model of a CME as a cone. Assuming also a constant traveling speed, a simpler cone-model is described by Michałek et al. (2003). Applying their model on 72 asymmetric halo CMEs (observed with LASCO) they showed that the average corrected speeds only differ $\sim$ 20 % from the projected speeds. This is not so surprising, since for large cone-angles (they find an average cone angle of 120°), the edges of the CME cone have still a large component in the plane of the sky. Assuming a symmetric CME with cone-angle 120° erupting from the central meridian gives v_proj = $\cos(90 - (120/2))^\circ$ v_rad = $\cos 30^\circ$ v_rad $\approx$ 0.7 v_rad. Using the fact that most halo CMEs are not symmetric this implies v_proj $\geq$ 0.7 v_rad for wide halo CMEs.

CME propagation models very often superpose a density blob on a given background. Nevertheless, in spite of this, the essential physics of the CME phenomenon probably resides in the magnetic field or its associated current systems (Hudson & Cliver 2001; Chané et al. 2005), which we cannot observe so directly as we observe the mass itself. Recent progress has been made in determining the magnetic field orientation of CMEs deduced from their on-disk counterparts. For example the chirality of the pre-eruption filament is strongly correlated with the orientation of the magnetic field at L1 associated with the CME and hence can be used to predict the probability of a geomagnetic storm (Yurchyshyn et al. 2001). In addition to the importance of Hα and EUV images showing pre-eruption magnetic field structures, they are also useful for determining whether a halo CME is Earth-directed, even though we can still make mistakes especially when the first detection of the CME comes long after (or before) the solar signatures. It is thus essential to observe different manifestations of CMEs in different types of data. For an elaborate review on the current monitoring capabilities we refer to Hochedez et al. (2005).

It is empirically (e.g. Crooker & Cliver 1994) and numerically (e.g. Odstrčil & Pizzo 1999) shown that the motion and appearance of a CME in interplanetary space is strongly affected by its interaction with the ambient heliospheric pattern. Besides, the combination of sequential CMEs can produce complex structures at 1 AU. It is thus important to include the influence of the background solar wind in the model. Some use the actual solar wind speed measured *in situ* as an approximation for the ambient wind speed. But the solar wind speed is a highly variable parameter and on the spatial and temporal timescale of an IP ejection it can vary as much as 100 km s^{-1} (e.g. Burlaga et al. 1987). Using such a value as model input can introduce in some cases larger errors than using an average wind speed (Vršnak & Gopalswamy 2002). The Wang-Sheeley-Arge (WSA) model (Wang & Sheeley 1992; Arge & Pizzo 2000) provides the background solar wind up to 1 AU extrapolating the photospheric magnetic field into the heliosphere using the potential field source surface (PFSS) model (Schatten et al. 1969; Altschuler & Newkirk 1969). It works quite well regarding the simplifying assumptions.

The open data policy common to solar physics makes a large quantity of data available, but some, e.g. LASCO (Large Angle and Spectrometric Coronagraph; Brueckner et al. 1995), are truly unique and therefore critical. On the other hand, some observations of great monitoring value are not easily or regularly accessible due to organizational problems. At the moment CMEs and their by-products are monitored by a number of different people independently, each one limited to its own instruments and specialization. As a consequence, their results remain

usually disconnected. The challenge now is to link the sparse observations from instruments distributed worldwide and in space missions, in order to develop a global approach to CME monitoring. New internet technologies such as the various grid efforts: EGSO (Bentley 2002); VSO (Davey et al. 2003); coSEC (Hurlburt et al. 2004) might greatly contribute to this attempt.

3 Existing software for automated CME detection in remote sensing data

Early 2005, various algorithms for the detection of CME manifestations are either up and running or under development. Depending on the targeted CME manifestation, different types of data are 'scanned' by automated procedures. Automated software has the ability of analyzing data continuously (i.e. 24hr/day) and objectively. Its implications for forecasting are twofold: (1) The software tools can send out near-real-time alerts to the solar and space weather community reporting on the detection and providing important CME characteristics. These details together with observations enable the forecaster to send out timely space weather warnings. However, the limited range $(0 - 32R_{\odot})$ of early CME observations limits the accuracy of these 2-4 day predictions. (2) Automatically generated alerts could also launch data-driven models simulating the response of the solar wind or the magnetosphere to the reported disturbance. For this purpose the automated software packages should calculate the most important parameters at 1 AU such as the solar wind bulk speed and density, ion temperature and magnetic field strength and orientation. to feed the model with a real-time disturbance. Hence the benefit of automated monitoring exceeds the level of immediate response, but can act as the 'missing link' between observation and modelling. In what follows we describe the existing detection algorithms on events linked to CME occurrence. Several of these techniques have been described in Robbrecht & Berghmans (2005) focussing on image processing.

3.1 Flare detection in X-ray and EUV data

A CME is often (but not always!) accompanied by a flare, a 'large' and 'sudden' increase in radiation, mostly in X-rays and ultraviolet wavelengths observed in image and irradiance data (see e.g. Hochedez et al. 2005). SXI (Solar X-ray Imager) observations from GOES-12 (the 12^{th} Geostationary Operational Environmental Satellite) provide valuable flare location and other information, especially when no optical (i.e. white light) observations are available. SEC (Space Environment Center) developed the SXI flare algorithm, triggered by GOES X-ray events, which finds the brightest area in the latest SXI image and assigns the region number of the closest active solar region. Since Jan. 2004 this information (XFL) is added to the Edited Solar Events Lists available online (http://www.sec.noaa.gov/ftpdir/indices/events/events.txt). It groups several reports into a single event, as determined by the SEC forecaster. It includes information on radio bursts, filament disappearances and prominence eruptions, flares in Hα and even Forbush decreases. However, due to human interference the SEC reports are sometimes lagging behind. Therefore, fully automated software developed for flare-monitoring form a valuable addition to this such as the SolarSoft Latest Events page (http://www.lmsal.com/solarsoft/latest_events/). X-ray flux enhancements above the B-class flare level are recorded automatically from GOES-10 irradiance data. For every flare a detailed page is setup providing the start- peak- and end-time of the flare and also its peak-intensity. The software also determines its location on the disk using EIT high cadence wavelength or SXI (GOES12) movies.

In the frame of their automatic alerting system the 'Solar Influences Data analysis Center' (Berghmans et al. 2005) has developed software to automatically detect flares, using GOES-12 irradiance data as input. The detector has been tuned as to produce the same flare parameters as NOAA/SEC. First tests (few tens of examples) show that the output is indeed identical to the NOAA/SEC flare report. The output is an ASCII table listing in a line per flare, its main parameters. It is also available online (http://sidc.oma.be/GOESdata).

3.2 Disappearing filaments in Hα

Over the last five years a number of groups successfully developed codes and algorithms for the automated detection of filaments, best observed in Hα images, where they appear as dark elongated threads. There exist different levels in output. The first detection schemes (Gao et al. 2002; Shih & Kowalski 2003; Fuller & Aboudarham 2004; Zharkova et al. 2003) generate black-and-white images with the black areas indicating the filaments. Besides a graphical display this allows determination of parameters like total filament area (pixel area) and location on the disk (e.g. coordinates of center of mass). This parameterized 'filament description' is important in view of automated interpretation of these outputs. However the above mentioned references do not report on the generation of output-tables containing relevant filament parameters. Automated filament detection schemes have to deal with a number of subproblems: finding the right intensity threshold, developing appropriate preprocessing techniques optimized for filament tracking, merging filament parts

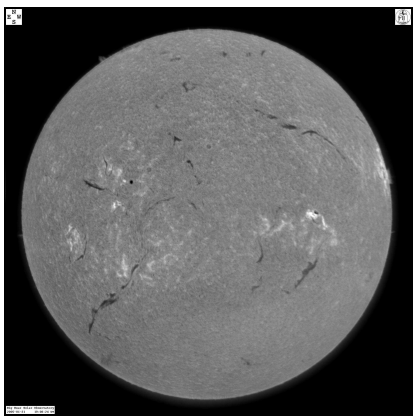

a. Hα image
(Image credit: BBSO)

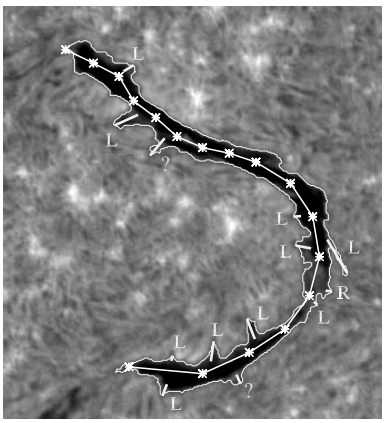

b. filament detection
(Image credit: P. Bernasconi; With kind permission of Springer Science and Business Media.)

Figure 2: *a:* Example of an processed Hα image from the Big Bear Solar Observatory (BBSO). Standard BBSO processing includes dark current and flat field correction, contrast enhancement and limb darkening removal. *b:* Example of a filament detection by Bernasconi & Rust, indicating the spine and barbs. Next to each barb is a letter indicating whether it is left-bearing (L), right-bearing (R) or undetermined (?). Since this filament has more left-bearing barbs than right-bearing ones, the code determines it to have sinistral chirality.

belonging to the same body, etc. These are extensively discussed in Robbrecht & Berghmans (2005). For space weather purposes, we are interested in filament disappearances. This implies that the technique is able to 'recognize' a filament in subsequent images. Very recently Qu et al. (2005) and Bernasconi et al. (2005) introduced spines to characterize the filaments. A Spine marks the 'skeleton' of a filament consisting of several footpoints mutually connected. Qu et al. (2005) use adaptive edge linking (introduced by Shih & Cheng 2004) to trace the filament's spine. Based on evolution in size and intensity a filament is reported to have disappeared or significantly shrunk. Bernasconi et al. (2005) apply a principal curve algorithm to find the spine; this is a multi-step iterative technique developed from Kégl's algorithm (Kégl et al. 2000). For every filament and in every image a central latitude and longitude is determined. If there is no close match for these coordinates in subsequent images, the filament is regarded as (partially) disappeared. Important to note here is the difference between thermal disappearance (DBt) and dynamical disappearance (DBd) (Mouradian et al. 1995). Only the latter one involves plasma ejections and leads to the permanent disappearance of filaments. Bernasconi et al. (2005) tersely take this into account by only allowing the label 'disappeared' for filaments that are not detected during 3 subsequent days. This limits of course its value for space weather warnings.

Analyses of Hα filaments and photospheric magnetograms have revealed two chiralities of filaments, dextral and sinistral (Martin et al. 1994). It can be determined using the orientation of barbs relative to the filament's main axis (Pevtsov et al. 2003). Using this technique Bernasconi et al. (2005) automatically determine a filaments' chirality and list it with the other filament parameters (see Fig.2). Chirality is an important parameter, since together with solar magnetic field data (e.g. MDI) the filaments' magnetic helicity can be determined. Under assumption of magnetic helicity conservation this means the polarity of the associated ICME can be estimated. Many observational studies report on this correlation (e.g. Bothmer & Schwenn 1994; McAllister et al. 2001; Yurchyshyn et al. 2001). These findings mean a great step forward in the predictability of the geoeffectiveness of the related CME.

The above described methods are applied on Hα observations from Big Bear Solar Observatory (BBSO, California) and the Meudon Observatory (in France). They are part of the global high resolution Hα network (http://www.bbso.njit.edu/Research/Halpha/).

3.3 prominence eruptions in radio images

Unique observations of solar eruptions are acquired with the Nobeyama Radio-heliograph-NoRH (Nakajima et al. 1995) at the National Astronomical Observatory of Japan since April, 1992. During the daily 8-hours of observations (from 23 to 07 UT), full disk solar images are produced at the 17GHz and 34 Ghz radio frequencies. In what follows we only consider the 17Ghz images which have a spatial resolution of 15 arcsec and a time resolution of 10 min (but they

are reconstructible down to a 50 ms resolution).

An operational tool was developed to detect so-called limb-events, including mostly prominence eruptions but also prominence activity and limb flares. The technique tracks the center of mass of bright pixel groups (off-limb) in subsequent images. If the group is detected in three subsequent images, the structure is defined as an event and listed on the website (http://solar.nro.nao.ac.jp/norh/html/prominence/).
The detection program runs once per day after the daily observation period (at 9 UT), after which the output is checked manually. Bad detections are removed from the list. The output per event contains the start-, peak- and end-time, the location of the event in cartesian coordinates and a rough estimate of its pixel-size. No velocity is measured, although Mouradian et al. (1995) report that speeds from radio data show good correspondence with CME speeds in initial phase.

3.4 EIT waves and dimmings

After the discovery of the so-called 'EIT wave' phenome-non Thompson et al. (1998) it was soon realised that these waves are strongly associated with earth-directed CMEs (e.g. Plunkett et al. 1998; Biesecker et al. 2002). A dimming is usually observed behind an EIT wave and is most likely due to the evacuation of mass during the CME (Thompson et al. 1998; Harra & Sterling 2001). Automatization of EIT wave detection is a hard problem given their large variety in physical appearance and their weak intensity variation. Recently Podladchikova & Berghmans (2005) developed software to automatically detect these EIT waves, illustrated in Fig.3. Bearing in mind the above mentioned problems, the detection is based on the characteristics of the histogram-distribution of running difference images. The presence of large-scale coherent structures, such as dimmings and EIT waves, strongly influences the higher order moments (skewness, kurtosis) of the distribution. Deviations therein can be used as triggers for the occurrence of an EIT wave and associated dimming. Its output is location, timing, structure and dynamics of the EIT wave.

3.5 CMEs in coronagraphic white light images

The classical white-light picture of a CME is that of a bright leading edge followed by a dark cavity and a central core representing the erupted prominence (Hundhausen et al. 1987). However, CMEs are very variable in appearance and often do *not* show clearly this three part structure. This is particularly true for halo CMEs, when the erupted matter is seen around the entire occulting disk. Automated detection and measurements of their physical properties (speed, density, mass, magnetic field) is therefore difficult. Berghmans et al. (2002) developed software which automatically detects CME propagations in coronagraphic image sequences. Instead of making morphology assumptions, this technique basically detects bright ridges in [time,height]-maps (see Sheeley et al. 1999) indicating features moving radially outward from the Sun. Recently (Robbrecht & Berghmans 2004) have enhanced the performance significantly; 96% of all CMEs during a 6 day test-period was recovered. The program now runs near-real-time ant the results are put immediately on-line. The output includes the first time of occurrence in the c2 field-of-view, a linear speed estimation, principal angle and angular width. An illustration can be found in Fig.4. The software sends out alerting messages whenever a partial halo CME candidate is detected.

4 Conclusions

Early 2005, we are on the eve of a new era in space weather forecasting, in which intelligent software may autonomously detect significant space weather events, launch model simulations and sends out warnings. This invokes incorporating real-time data-driven models in the forecasting process. Existing efforts on magnetospheric data-driven models serve as valuable examples. The next step towards automated space weather forecasting is to fill the data gap between early observations of a CME and its *in situ* manifestation using CME propagation models. We have argued than this can greatly improve the accuracy when forecasting the space weather a few days ahead. Hence, CME surveillance implies defining CME and ambient solar wind parameters, which can serve as input for data-driven models. We believe that only automated CME detection software is able to deliver these parameters in a timely manner.

We have given an overview of the existing software for automated CME detection. Their output parameters are valuable for both, the space weather forecaster and the models simulating the propagation of the detected CME. Hence the benefit of automated monitoring exceeds the level of immediate response, but can act as the 'missing link' between observation and modelling.

To ensure the success of the model-for-forecasting principle a collaborative effort is needed from both, the automated detection community and the CME modelling community. The detection software have to be tuned in order to deliver the required inputs in a computer-readable format.

References

Altschuler, M. D. & Newkirk, G. 1969, Sol. Phys., 9, 131

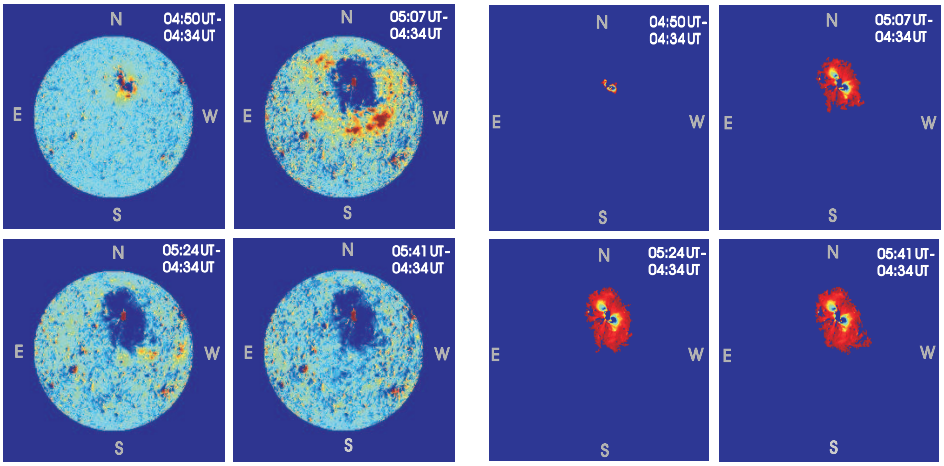

a. Base difference images b. Extracted dimming

Figure 3: Illustration of a dimming extraction on EIT 195$\mathring{A}$ running difference images on 12 May 1997, by Podladchikova & Berghmans (2005)(see this paper for a color version). After a dimming is detected its location and size is found by applying a region growing method. [Image credit: E. Podladchikova; With kind permission of Springer Science and Business Media.]

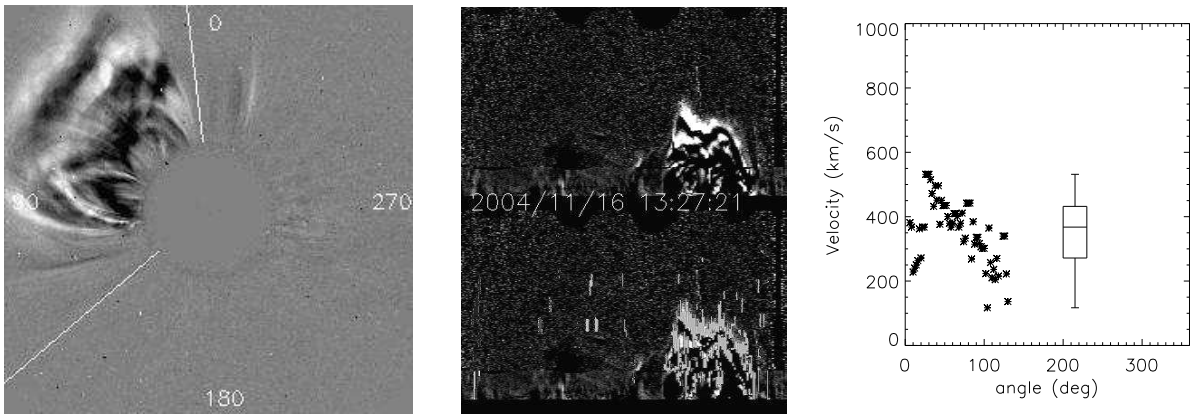

a. C2 Running difference b. polar transformed c. CME speed

Figure 4: Illustration of a CME detection by CACTus (for a color illustration see Robbrecht & Berghmans, 2004). *a:* C2 running difference image, the white lines indicate the measured angular width of the CME. *b:* The CME in polar view. The top panel shows the original running difference image. The bottom panel shows the CACTus CME detection. *c:* CME velocity profile as a function of the angle, which runs counterclockwise from the north. A boxplot is drawn: the box itself contains the middle 50% of the measured speeds. The whiskers at both ends indicate respectively the minimal and maximal detected speeds. Note that the whiskers are no error-bars, but indicate the range of the measured speeds.

Arge, C. N. & Pizzo, V. J. 2000, J. Geophys. Res., 105, 10465

Bentley, R. D. 2002, in ESA SP-477: Solspa 2001, Proceedings of the Second Solar Cycle and Space Weather Euroconference, 603–606

Berghmans, D., Foing, B. H., & Fleck, B. 2002, in ESA SP-508: From Solar Min to Max: Half a Solar Cycle with SOHO, 437–440

Berghmans, D., Van der Linden, R., Vanlommel, P., et al. 2005, Annales Geophysicae,

Bernasconi, P. N., Rust, D. M., & Hakim, D. 2005, Sol. Phys., 228, 97

Biesecker, D. A., Myers, D. C., Thompson, B. J., Hammer, D. M., & Vourlidas, A. 2002, ApJ, 569, 1009

Bothmer, V. & Schwenn, R. 1994, Space Science Reviews, 70, 215

Brueckner, G. E., Howard, R. A., Koomen, M. J., et al. 1995, 162, 357

Burlaga, L. F., Behannon, K. W., & Klein, L. W. 1987, J. Geophys. Res., 92, 5725

Chané, E., Jacobs, C., van der Holst, B., Poedts, S., & Kimpe, D. 2005, A&A, 432, 331

Cliver, E. W. & Hudson, H. S. 2002, Journal of Atmospheric and Terrestrial Physics, 64, 231

Crooker, N. U. & Cliver, E. W. 1994, J. Geophys. Res., 99

dal Lago, A., Schwenn, R., & Gonzalez, W. D. 2003, Advances in Space Research, 32, 2637

Davey, A. R., Bogart, R. S., Dimitoglou, G., et al. 2003, AAS/Solar Physics Division Meeting, 34

Defise, J., Halain, J., Mazy, E., et al. 2001, in Proc. SPIE Vol. 4498, p. 63-72, UV/EUV and Visible Space Instrumentation for Astronomy and Solar Physics, Oswald H. Siegmund; Silvano Fineschi; Mark A. Gummin; Eds., 63–72

Eyles, C. J., Simnett, G. M., Cooke, M. P., et al. 2003, Sol. Phys., 217, 319

Forbes, T. G. 2000, J. Geophys. Res., 23153

Fuller, N. & Aboudarham, J. 2004, Lecture notes in computer science

Gao, J., Wang, H., & Zhou, M. 2002, Sol. Phys., 205, 93

Gopalswamy, N. 2003, EGS - AGU - EUG Joint Assembly, Abstracts from the meeting held in Nice, France, 6 - 11 April 2003, abstract #4456, 4456

Gopalswamy, N., Yashiro, S., Liu, Y., et al. 2005, Journal of Geophysical Research (Space Physics), 110, 9

Gosling, J. T., Hildner, E., MacQueen, R. M., et al. 1974, J. Geophys. Res., 79, 4581

Gosling, J. T., McComas, D. J., Phillips, J. L., et al. 1994, Geophys. Res. Lett., 21, 2271

Gosling, J. T., Thomsen, M. F., Bame, S. J., Elphic, R. C., & Russell, C. T. 1990, Geophys. Res. Lett., 17, 2245

Harra, L. K. & Sterling, A. C. 2001, ApJ, 561, L215

Hochedez, J.-F., Zhukov, A., Robbrecht, E., et al. 2005, Annales Geophysicae

Hudson, H. S. & Cliver, E. W. 2001, J. Geophys. Res., 25199

Hundhausen, A. J., Holzer, T. E., & Low, B. C. 1987, J. Geophys. Res., 92, 11173

Hurlburt, N., Bose, P., Freeland, S., Woodward, M., & Slater, G. 2004, American Astronomical Society Meeting Abstracts, 204

Intriligator, D. S., Sun, W., Dryer, M., et al. 2005, Journal of Geophysical Research (Space Physics), 110, 9

Kégl, B., Krzyżak, A., Linder, T., & Zeger, K. 2000, IEEE Transactions on Pattern Analysis and Machine Intelligence

Low, B. C. 2001, J. Geophys. Res., 25141

Low, B. C. & Zhang, M. 2002, ApJ, 564, L53

Luhmann, J. G., Solomon, S. C., Linker, J. A., et al. 2004, Journal of Atmospheric and Terrestrial Physics, 66, 1243

Manchester, W. B., Gombosi, T. I., Roussev, I., et al. 2004, Journal of Geophysical Research (Space Physics), 2107

Martin, S., Billimoria, R., & Tracadas, P. 1994, in Solar Surface Magnetism, 303

McAllister, A. H., Martin, S. F., Crooker, N. U., Lepping, R. P., & Fitzenreiter, R. J. 2001, J. Geophys. Res., 29185

Michałek, G., Gopalswamy, N., & Yashiro, S. 2003, ApJ, 584, 472

Mouradian, Z., Soru-Escaut, I., & Pojoga, S. 1995, Sol. Phys., 158, 269

Munro, R. H., Gosling, J. T., Hildner, E., et al. 1979, Sol. Phys., 61, 201

Nakajima, H., Nishio, M., Enome, S., et al. 1995, Journal of Astrophysics and Astronomy Supplement, 16, 437

Odstrcil, D., Riley, P., & Zhao, X. P. 2004, Journal of Geophysical Research (Space Physics), 109, 2116

Odstrčil, D. & Pizzo, V. J. 1999, J. Geophys. Res., 104, 493

Pevtsov, A. A., Balasubramaniam, K. S., & Rogers, J. W. 2003, ApJ, 595, 500

Plunkett, S. P., Thompson, B. J., Howard, R. A., et al. 1998, Geophys. Res. Lett., 25, 2477

Podladchikova, O. & Berghmans, D. 2005, Sol. Phys., 228, 265

Qu, M., Shih, F. Y., Jing, J., & Wang, H. 2005, Sol. Phys., 228, 119

Robbrecht, E. & Berghmans, D. 2004, A&A, 425, 1097

Robbrecht, E. & Berghmans, D. 2005, Sol. Phys., 228, 239

Schatten, K. H., Wilcox, J. M., & Ness, N. F. 1969, Sol. Phys., 6, 442

Schwenn, R., Dal Lago, A., Gonzalez, W. D., et al. 2001, AGU Fall Meeting Abstracts, A739+

Sheeley, N. R., Walters, J. H., Wang, Y.-M., & Howard, R. A. 1999, J. Geophys. Res., 104, 24739

Shih, F. Y. & Cheng, S. 2004, Information sciences, 167, 9

Shih, F. Y. & Kowalski, A. J. 2003, Sol. Phys., 218, 99

Spence, H., Baker, D., Burns, A., et al. 2004, Journal of Atmospheric and Terrestrial Physics, 66, 1499

Thompson, B. J., Plunkett, S. P., Gurman, J. B., et al. 1998, Geophys. Res. Lett., 25, 2465

Tousey, R., Howard, R. A., & Koomen, M. J. 1974, BAAS, 6, 295

Tsurutani, B. T., Gonzalez, W. D., Kamide, Y., & Arballo, J. K. 1997, Preface (Magnetic Storms, Geophysical Monograph Series, Vol. 98), D9+

Vršnak, B. & Gopalswamy, N. 2002, Journal of Geophysical Research (Space Physics), 107, 2

Wang, Y.-M. & Sheeley, N. R. 1992, ApJ, 392, 310

Watanabe, T. & Schwenn, R. 1989, Space Science Reviews, 51, 147

Wu, S. T. & Guo, W. P. 1999, Journal of Atmospheric and Terrestrial Physics, 61, 109

Xie, H., Ofman, L., & Lawrence, G. 2004, Journal of Geophysical Research (Space Physics), 109, 3109

Yurchyshyn, V., Wang, H., & Abramenko, V. 2003, Advances in Space Research, 32, 1965

Yurchyshyn, V., Wang, H., & Abramenko, V. 2004, Space Weather, 2, 2001

Yurchyshyn, V. B., Wang, H., Goode, P. R., & Deng, Y. 2001, ApJ, 563, 381

Zhang, J., Liemohn, M. W., Kozyra, J. U., Lynch, B. J., & Zurbuchen, T. H. 2004, Journal of Geophysical Research (Space Physics), 9101

Zhao, X. P., Plunkett, S. P., & Liu, W. 2002, Journal of Geophysical Research (Space Physics), 107, 13

Zharkova, V. V., Ipson, S. S., Zharkov, S. I., et al. 2003, Sol. Phys., 214, 89